

Spin-orbit coupling and operation of multivalley spin qubits

M. Veldhorst,^{1,*} R. Ruskov,² C. H. Yang,¹ J. C. C. Hwang,¹ F. E. Hudson,¹ M. E. Flatté,³ C. Tahan,²
K. M. Itoh,⁴ A. Morello,¹ and A. S. Dzurak^{1,†}

¹*Centre for Quantum Computation and Communication Technology, School of Electrical Engineering and Telecommunications,
The University of New South Wales, Sydney NSW 2052, Australia*

²*Laboratory for Physical Sciences, 8050 Greenmead Drive, College Park, Maryland 20740, USA*

³*Department of Physics and Astronomy, University of Iowa, Iowa City, Iowa 52242, USA*

⁴*School of Fundamental Science and Technology, Keio University, 3-14-1 Hiyoshi, Kohoku-ku, Yokohama 223-8522, Japan*

(Received 5 May 2015; revised manuscript received 15 October 2015; published 5 November 2015)

Spin qubits composed of either one or three electrons are realized in a quantum dot formed at a Si/SiO₂ interface in isotopically enriched silicon. Using pulsed electron-spin resonance, we perform coherent control of both types of qubits, addressing them via an electric field dependent g factor. We perform randomized benchmarking and find that both qubits can be operated with high fidelity. Surprisingly, we find that the g factors of the one-electron and three-electron qubits have an approximately linear but opposite dependence as a function of the applied dc electric field. We develop a theory to explain this g -factor behavior based on the spin-valley coupling that results from the sharp interface. The outer “shell” electron in the three-electron qubit exists in the higher of the two available conduction-band valley states, in contrast with the one-electron case, where the electron is in the lower valley. We formulate a modified effective mass theory and propose that intervalley spin-flip tunneling dominates over intravalley spin flips in this system, leading to a direct correlation between the spin-orbit coupling parameters and the g factors in the two valleys. In addition to offering all-electrical tuning for single-qubit gates, the g -factor physics revealed here for one-electron and three-electron qubits offers potential opportunities for different qubit control approaches.

DOI: [10.1103/PhysRevB.92.201401](https://doi.org/10.1103/PhysRevB.92.201401)

PACS number(s): 85.35.Gv, 03.67.Lx, 81.07.Ta

Silicon is known to have small spin-orbit coupling (SOC), a beneficial fact for silicon quantum computing, since charge noise is largely decoupled from information stored in the spin [1]. Furthermore, silicon can be isotopically enriched and chemically purified to ²⁸Si, thereby removing nuclear-spin background fluctuations and so silicon is often referred to as a semiconductor vacuum [2]. These two facts have motivated intense research on silicon qubits, leading to recent realizations of single-qubit [3–7] and two-qubit [8] logic gates. Despite the small SOC, the tunability of the g factor via gate-controlled electric fields allows one to electrostatically turn on and off the spin rotations that constitute single-qubit gates [7–9], thereby providing an important tool for quantum computation.

The low-energy subspace in silicon quantum dot (QD) systems is governed by two spin-degenerate valley states. When these valley states are quasidegenerate, qubit operation becomes complex [6], and coupling qubits is even more challenging [10]. However, the valley states can be separated using a vertical electric field and the sharp potential of an interface, and their energy separation can be electrically controlled over several hundreds of μeV [7,11]. While one-electron spin qubits are naturally operated in the lowest valley state [6,7], it is intriguing to consider the performance of qubits operated in the higher valley state, which has a long spin lifetime when orbital relaxation is suppressed [11]. When spatial confinement in the QD is strong, the orbital excited states are lifted high in energy and qubit operation in the upper valley state is possible by populating three electrons in the quantum dot, assuming a single-particle description (see, e.g.,

Refs. [10,12]). In this mode two electrons form a singlet in the lower valley state and the third electron is operated in the upper valley [see Figs. 1(a) and 1(b)]. It has been suggested that such multielectron qubits could enhance the gate fidelity, due to partial screening of electrical noise [13].

Here we study the valley structure of silicon and spin-orbit coupling by high-fidelity operation of one- and three-electron spin qubits, operated in the lower and upper valley, respectively. Using electron-spin resonance (ESR) we map out the qubit frequency as a function of the applied perpendicular electric field. We experimentally demonstrate and theoretically explain how inter-valley spin-orbit coupling at the Si/SiO₂ interface results in an opposite dependence of the g factor for the two valleys. Via the direct g -factor coupling to the electric field the three-electron (upper valley) qubit is about twice as sensitive to external field fluctuations compared to the one-electron qubit, leading to a different decoherence mechanism than discussed in Ref. [13] and resulting in a lower three electron-qubit fidelity. Randomized benchmarking supports this observation, while showing that both qubit systems are capable of fidelities above 99%, approaching the surface code thresholds for fault-tolerant quantum computing [14].

The QD structure is fabricated on an epitaxially grown, isotopically purified ²⁸Si epilayer with a residual concentration of ²⁹Si at 800 ppm [2] using multilevel gate stack silicon metal-oxide-semiconductor (Si MOS) technology [15]; see Fig. 1. The charge stability diagram of the quantum dot is shown in Fig. 1(c). From a Ramsey sequence on the three-electron qubit (see Fig. 2) we find a dephasing time $T_2^* = 70 \mu\text{s}$, which is slightly less than we have previously measured for the one-electron qubit, which had $T_2^* = 120 \mu\text{s}$ [7].

We have demonstrated electric-field control over the resonance frequency ν_{ESR} of the one-electron qubit [7], showing

*M.Veldhorst@unsw.edu.au

†A.Dzurak@unsw.edu.au

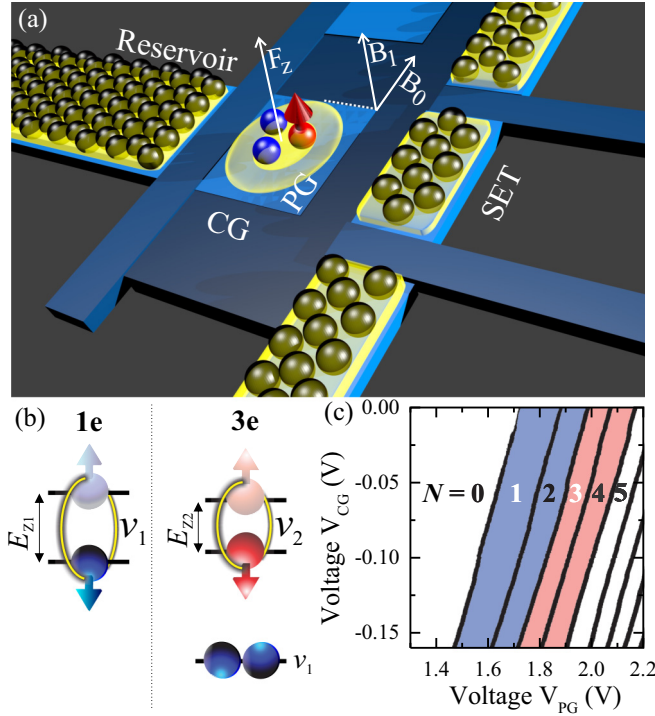


FIG. 1. (Color online) (a) Schematic representation of the quantum dot system. The quantum dot is defined using the confinement gate CG and plunger gate PG and the yellow shading represents the regions where electrons are accumulated, with F_z the perpendicular electric field direction. ESR control is via a dc magnetic field $B_0 = 1.4$ T (in the Si [110] in-plane direction) and an ac magnetic field B_1 . (b) The quantum dot qubit can be operated using the spin states of one electron, or using three electrons, where two electrons (blue) occupy the lowest energy valley state and the third electron (red) is in the higher energy valley state. (c) Charge stability diagram showing the electron occupancy N in the quantum dot, measured with a nearby SET.

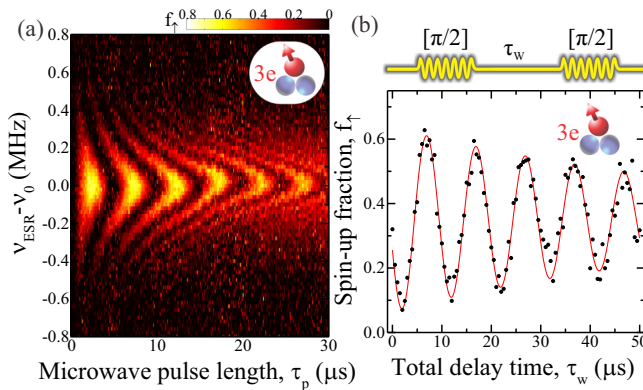


FIG. 2. (Color online) Demonstration of qubit control of the three-electron qubit. (a) 2D color map showing Rabi control of the spin-up fraction f_{\uparrow} , by varying the microwave pulse length and the microwave driving frequency ν_{ESR} . We have subtracted a reference frequency $\nu_0 = 39.045$ GHz (corresponding to $g = 1.9908$) for clarity. (b) Ramsey fringes, obtained by varying the waiting time between two ESR $\pi/2$ pulses. The decay in the spin-up fraction f_{\uparrow} corresponds to $T_2^* = 70$ μ s. The confinement gate voltage is $V_C = -0.2$ V.

tunability over several MHz that appears linear in electric field, corresponding to more than 3000 times the 2.4-kHz ESR linewidth. We find that spin-valley mixing of the QD eigenstates due to interface (local) roughness [11] would predict a modification of the electron g factor that is two orders of magnitude smaller than is found experimentally, together with a nonlinear dependence close to the anticrossing point of the spin-valley states that we do not observe.

Here we propose and analyze a model where the g -factor modification proceeds via intervalley spin-flip tunneling, mediated by the strong z confinement at the interface. The Si/SiO₂ (001) interface of silicon MOS quantum dots can be described with a Hamiltonian that consists of a bulk term \mathcal{H}_0 and an interface term \mathcal{H}_{if} . The reduction of the bulk Si crystal symmetry at the interface, in the presence of strong perpendicular electron confinement induced by an applied electric field F_z , lifts the sixfold valley degeneracy, leaving two low-lying Δ valleys at $\pm k_{0z}$. These are then mixed via enhanced intervalley tunneling due to the strong z confinement at the interface [16,17]. The consequent effective two-valley Hamiltonian acts on the four-component vector $[\Phi_{z,\uparrow}(r), \Phi_{z,\downarrow}(r), \Phi_{-z,\uparrow}(r), \Phi_{-z,\downarrow}(r)]^T \equiv \Phi(r)$, where the bulk part (spin and valley degenerate) is given by

$$\mathcal{H}_0 = \left[\sum_{j=x,y,z} \frac{\hbar^2 \hat{k}_j^2}{2m_j} + U_{x,y} + U_z \right] \times \hat{I}_4 \quad (1)$$

with the quasimomentum operators $\hat{k}_j \equiv -i\partial_j$; and $U_{x,y} = \frac{m_t}{2}\omega_0^2(x^2 + y^2)$ and $U_z = |e|F_z z$ are the in-plane and perpendicular confinement electron potentials, respectively. Here m_t , m_l are the Si effective Δ -valley electron masses, $|e|$ is the electron charge, and \hbar is the reduced Planck constant. Taking into account the large band offset of Si/SiO₂, the interface term is

$$\mathcal{H}_{\text{if}} = -\frac{\hbar^2}{2Rm_l}\delta(z-z_0) - i\frac{\hbar^2}{2m_l}\delta(z-z_0)\hat{k}_z + \delta(z-z_0)\hat{V}_{\text{if}}(\mathbf{k}), \quad (2)$$

where R is a parameter with dimension of length, characterizing an abrupt interface [18,19], and $|R| \ll l_z \ll l_D$; here $l_z = (\hbar^2/2m_l|e|F_z)^{1/3}$ and $l_D = (\hbar/m_t\omega_0)^{1/2}$ are the perpendicular and in-plane confinement lengths (assuming much stronger \hat{z} confinement). For $R \approx 0$ the interface Hamiltonian [Eq. (2)] corresponds to the standard infinite boundary condition (BC) $\Phi(z)|_{z=z_0} = 0$, while for finite R it generates spin and valley mixing at the interface, also preserving the hermiticity of the Hamiltonian in the half space [18,20], $z \gtrsim z_0$. Following the symmetry reasoning of Refs. [21,22] the spin-valley mixing interface matrix $\hat{V}_{\text{if}}(\mathbf{k})$ can be expressed via the C_{2v} invariants $H_R(\mathbf{k}) = \sigma_x k_y - \sigma_y k_x$, $H_D(\mathbf{k}) = \sigma_x k_x - \sigma_y k_y$, resulting in

$$\hat{V}_{\text{if}}(\mathbf{k}) = \begin{bmatrix} A(\mathbf{k}) & V\hat{I}_2 + B(\mathbf{k}) \\ V^*\hat{I}_2 + B^\dagger(\mathbf{k}) & A(\mathbf{k}) \end{bmatrix}. \quad (3)$$

In Eq. (3) the 2×2 block-diagonal element $A(\mathbf{k}) \equiv s_D H_D(\mathbf{k}) + s_R H_R(\mathbf{k})$ corresponds to *intravalley* spin-flipping transitions, while the off-diagonal elements are related to *intervalley* tunneling (in momentum space) with no

spin-flipping amplitude $V \equiv |V|e^{i\phi_V}$ with phase [22,23], or with a spin-flipping process, $B(\mathbf{k}) \equiv \chi_D H_D(\mathbf{k}) + \chi_R H_R(\mathbf{k})$.

Since experimentally the valley splitting ($\sim|V|$) is generally large with respect to the spin-flipping terms, we diagonalize with respect to the leading V -matrix element and via a unitary transformation we find

$$\hat{V}_{\text{if}}^U(\mathbf{k}) = \begin{bmatrix} |V| + A + \frac{1}{2}B_d & \frac{1}{2}B_{\text{off}} \\ \text{H.c.} & -|V| + A - \frac{1}{2}B_d \end{bmatrix}. \quad (4)$$

This matrix is approximately diagonal in the valley basis $|v_1\rangle$, $|v_2\rangle$, with a calculated valley splitting energy $E_{\text{VS}} = 2|V|R^2|\varphi'(0)|^2 = 2|V|R^2l_z^{-3} \propto F_z$. We neglect the off-diagonal contribution $B_{\text{off}} \equiv B - B^\dagger e^{2i\phi_V}$ in Eq. (4), since it is suppressed as $\sim 1/E_{\text{VS}}$ and E_{VS} is typically several hundreds of μeV in MOS quantum dots [7,11]. Thus, in the valley subspaces $|v_1\rangle$, $|v_2\rangle$, one can consider two independent boundary conditions as in Eq. (2), with spin-flipping interface matrices $\hat{V}_{v_1,v_2} = A \mp \frac{1}{2}B_d \equiv A \mp \frac{1}{2}(Be^{-i\phi_V} + B^\dagger e^{i\phi_V})$, in which the intervalley spin-flip tunneling element changes sign between v_1 and v_2 .

The effective two-dimensional (2D) spin-orbit Hamiltonians [proportional to the Rashba and Dresselhaus forms, $H_R(\mathbf{k})$, $H_D(\mathbf{k})$] are calculated by recasting the BC, Eq. (2), to a standard one via a suitable unitary transform, $\hat{\Phi}|_{z=z_0} \equiv \hat{\Gamma}_{\text{bc}}\Phi|_{z=z_0} = 0$, and obtaining a smooth perturbing Hamiltonian: $\delta\mathcal{H} \simeq R^2 \frac{2m_l}{\hbar^2} \hat{V}_{\text{if}}(k) \partial_z U_z$.

The corresponding 2D SOC parameters change due to sign flipping:

$$\begin{aligned} \alpha_{R;v_1,v_2} &= [s_R \mp |\chi_R| \cos(\phi_R - \phi_V)] R^2 |\varphi'(0)|^2, \\ \beta_{D;v_1,v_2} &= [s_D \mp |\chi_D| \cos(\phi_D - \phi_V)] R^2 |\varphi'(0)|^2. \end{aligned} \quad (5)$$

The scaling of the spin-orbit terms with the electric field F_z is linear, as is the valley splitting, E_{VS} . Here, we have introduced the phases ϕ_R and ϕ_D for the Rashba and Dresselhaus terms and $\varphi'(0)$ is the derivative of the z component of an eigenstate of the bulk Hamiltonian \mathcal{H}_0 . These results are similar to the strong-field limit results of Ref. [22].

Explicit calculation of the g -factor change, based on the interface Hamiltonian Eq. (2) and the fact that an in-plane magnetic field mixes the perpendicular and in-plane motion, shows that the in-plane interface g -factor renormalization δg^{if} is proportional to α_R , β_D ; nonparabolicity effects [24] are estimated to be much smaller, to be presented elsewhere. We find for the magnetic field parallel to the [110] direction

$$\delta g_{v_1,v_2}^{\text{if}} = -\frac{(\alpha_{R;v_1,v_2} - \beta_{D;v_1,v_2})|e|\langle z \rangle}{\hbar\mu_B}, \quad (6)$$

where μ_B is the Bohr magneton and $\langle z \rangle \simeq 1.5587l_z$ is an average of the z motion in the lowest subband; see Eq. (1). The g factor scales as $F_z^{2/3}$, which is close to a linear scaling over the range ($\sim 10\%$) of the experimentally applied electric fields; see Fig. 3(b).

We therefore expect from Eq. (6) that the renormalization δg will be of opposing sign for the two valleys, following the sign change of the SOC parameters in Eq. (5). In particular, the change will be exactly opposite for zero intravalley spin-flip

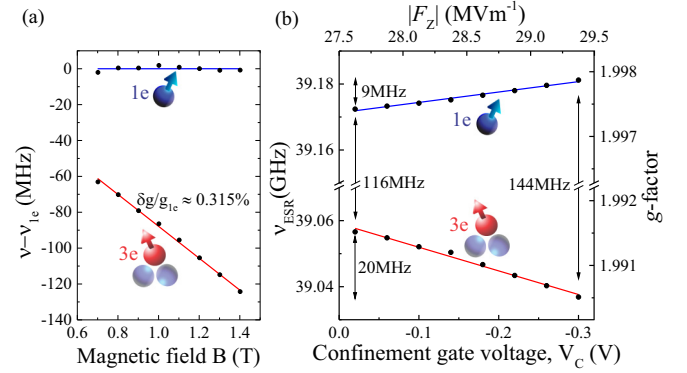


FIG. 3. (Color online) (a) Magnetic field dependence of the resonance frequency of the one- and three-electron qubit, with $F_z = 28.25$ MV/m. The experimental data of both qubit systems has been subtracted by the g_{1e} factor for comparison and we have calibrated the dc magnetic field using the crossing point of the one- and three-electron qubit resonance frequencies. We find $g_{1e} = 1.9975$ and $g_{3e} = 1.9912$. (b) Gate tuned electric field control over the valley g factor at $B_0 = 1.4015$ T.

coupling, $s_R, s_D = 0$:

$$\delta g_{v_1} = -\delta g_{v_2}. \quad (7)$$

Relatively smaller corrections due to nonzero intravalley spin flipping, $s_R, s_D \neq 0$, will generally violate Eq. (7), leaving the g -factor changes opposite in sign, but with different absolute value, $|\delta g_{v_1}| \neq |\delta g_{v_2}|$.

To observe this experimentally, we control the quantum dot electric field via the plunger gate PG and the confinement gate CG; see Fig. 1. In Fig. 3(a) we show the magnetic field dependence and in Fig. 3(b) we show electrical control over the qubit resonance frequency ν_{ESR} . The opposite electric-field dependence of the g factor for the two valleys is in qualitative agreement with the prediction of Eq. (7). Since the resonance frequency of the one-electron qubit increases with the electric field, while the resonance frequency of the three-electron qubit decreases [see Fig. 3(b)], we infer from Eq. (6) that the Rashba and Dresselhaus contributions are in this experiment subject to the constraints: $\delta\chi_{\text{interval}} \equiv |\chi_R| \cos(\phi_R - \phi_V) - |\chi_D| \cos(\phi_D - \phi_V) > 0$, $\delta s_{\text{interval}} \equiv s_R - s_D < 0$. The change in sign of δg is evidence that the intervalley spin-flip contributions dominate the intravalley spin-flip processes and from the δg dependence we estimate the ratio $\delta\chi_{\text{interval}}/|\delta s_{\text{interval}}| \approx 2.6$. This observation is consistent with tight-binding calculations on SiGe quantum wells [22], which predict that the intervalley transitions can be about an order of magnitude larger than the intravalley transitions. The values and signs of the SiGe parameters, as substituted in Eqs. (5) and (6), reproduce also the correct qualitative behavior of δg_{v_1} (δg_{v_2}) that increases (decreases) with the applied electric field F_z . However, the experimental ratio of the g -factor changes is $|\delta g_{v_2}|/|\delta g_{v_1}| \simeq 2.2$, while that calculated with the Si/SiGe parameters is ~ 1 . Such differences can be expected due to the greater band-edge offset in Si/SiO₂, disorder [25], and built-in electric fields.

In order to explore the qubit performance, we have performed (interleaved) randomized benchmarking (RB) [26,27] on the one-electron qubit [7] and three-electron qubit, and

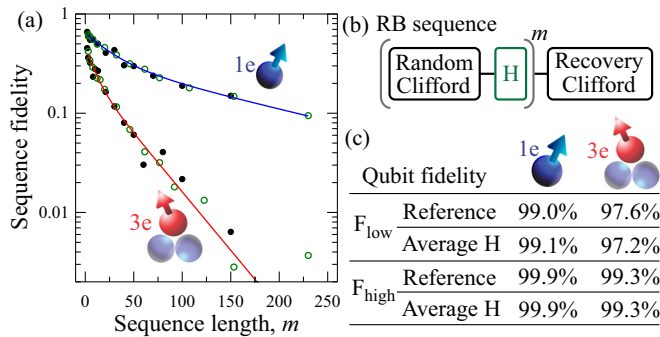


FIG. 4. (Color online) Clifford based randomized benchmarking. (a) Sequence fidelity as a function of the sequence length and (b) schematic representation of randomized benchmarking, where H is an interleaved test gate. In (a), the black filled circles correspond to standard randomized benchmarking and the green open circles to the average of the single qubit gates $[I, \pm X, \pm \frac{1}{2}X, \pm Y, \pm \frac{1}{2}Y]$, obtained by interleaved randomized benchmarking and normalizing the sequence length with $2.875/1.875$, such that it matches the average Clifford gate length. Both data sets are fitted with a two-fidelity model (see text) and the results are shown in (c), where the standard error is smaller than the corresponding gate error.

all results are shown in Fig. 4. In order to eliminate the fitting parameter B_{RB} , which is a constant offset parameter present in standard RB fits, we plot the sequence fidelity combination $F = F_{\uparrow} + F_{\downarrow} - 1$, which approaches zero for infinite sequence length when the assumptions of RB hold [28]. When the noise is gate independent, an exponential decay is expected. However, when low-frequency noise is present, nonexponential decays arise [28]. This nonexponential decay is due to slow drifts in the resonance frequency, such that the time ensemble is averaged over sequences with small detuning (resulting in a high fidelity, F_{high} , and a slow exponential decay) and large detuning (resulting in a low fidelity, F_{low} , and a fast exponential decay).

When such low-frequency noise is present, the fidelity varies over time and we use a two-fidelity model to analyze the data [28]. We have fitted the data using $F = A(p^m + q^m)$, where A quantifies the state preparation and measurement (SPAM) error and p and q are two polarization parameters. In Fig. 4(c) we show the corresponding fidelities. The three-electron qubit has a relatively low fidelity when the noise causes a large detuning ($F_{\text{low}} \approx 97\%$). However, when the microwave driving frequency is on resonance, both qubits have a fidelity above thresholds for fault tolerant quantum computing [14]; the average single-gate fidelity being $F_{\text{high}} =$

99.9% for the one-electron qubit system and $F_{\text{high}} = 99.3\%$ for the three-electron qubit system. While the three-electron qubit initially shows a nonexponential decay, for higher m the decay approaches a pure exponential, indicating that low-frequency noise has little impact in this range. We expect similar calibration errors for the one- and three-electron qubits, since the same setup is used. The exponential decay of the three-electron qubit is therefore likely due to high-frequency noise.

The faster decay of the sequence fidelity of the three-electron vs one-electron qubit is consistent with a larger sensitivity to electrical noise, as revealed by the larger frequency shift with gate voltage, $|\delta\nu_{3e}/\delta V| \approx 2.2|\delta\nu_{1e}/\delta V|$, shown in Fig. 3(b). The frequency detuning caused by electrical noise results in rotations around the z axis of the qubit Bloch sphere and perpendicular to the Rabi driving axis. In the small-angle approximation, this would result in an error rate that is around five times larger for the three-electron qubit, comparable with the difference in fidelities between the one-electron and three-electron qubits. It is therefore likely that both qubits are ultimately limited by high-frequency electrical noise, possibly due to charge noise from the aluminium-SiO₂ interface [29].

The realizations of single- and two-qubit gates using isotopically purified silicon quantum dots [7,8] are now revealing the early promises of silicon as a platform for quantum computation and the possibility of qubit operation with either one-electron or three-electrons allows more flexibility in scaling these systems. The ultranarrow spin-resonance linewidth of these qubits has pushed silicon into a regime where the weak spin-orbit coupling in silicon becomes not only visible, but also forms a different tool to control the spin states, as shown here. Further qubit optimization may be achieved by reducing the spin-orbit interaction, for example by changing the magnetic field amplitude or orientation, while the remarkably large electric-field control in Si MOS quantum dots provides additional motivation to explore spin-orbit coupling in silicon for qubit control and spin manipulation.

The authors thank L. M. K. Vandersypen for insightful discussions. The authors acknowledge support from the Australian Research Council (Grant No. CE110001027), the U.S. Army Research Office (Grant No. W911NF-13-1-0024), and the NSW Node of the Australian National Fabrication Facility. M.V. acknowledges support from the Netherlands Organization for Scientific Research (NWO) through a Rubicon Grant. The work at Keio has been supported in part by a Grant-in-Aid for Scientific Research by MEXT, in part by NanoQuine, in part by FIRST, and in part by JSPS Core-to-Core Program.

[1] F. A. Zwanenburg, A. S. Dzurak, A. Morello, M. Y. Simmons, L. C. L. Hollenberg, G. Klimeck, S. Rogge, S. N. Coppersmith, and M. A. Eriksson, *Rev. Mod. Phys.* **85**, 961 (2014).
 [2] K. M. Itoh and H. Watanabe, *MRS Commun.* **4**, 143 (2014).
 [3] B. M. Maune, M. G. Borselli, B. Huang, T. D. Ladd, P. W. Deelman, K. S. Holabird, A. A. Kiselev, I. Alvarado-Rodriguez, R. S. Ross, A. E. Schmitz, M. Sokolich, C. A. Watson, M. F. Gyure, and A. T. Hunter, *Nature (London)* **481**, 344 (2012).

[4] J. J. Pla, K. Y. Tan, J. P. Dehollain, W. H. Lim, J. J. L. Morton, D. N. Jamieson, A. S. Dzurak, and A. Morello, *Nature (London)* **489**, 541 (2012).
 [5] D. Kim, Z. Shi, C. B. Simmons, D. R. Ward, J. R. Prance, T. S. Koh, J. K. Gamble, D. E. Savaga, M. G. Lagally, M. Friesen, S. N. Coppersmith, and M. A. Eriksson, *Nature (London)* **511**, 70 (2014).
 [6] E. Kawakami, P. Scarlino, D. R. Ward, F. R. Braakman, D. E. Savage, M. G. Lagally, M. Friesen, S. N. Coppersmith, M. A.

- Eriksson, and L. M. K. Vandersypen, *Nat. Nanotechnol.* **9**, 666 (2014).
- [7] M. Veldhorst, J. C. C. Hwang, C. H. Yang, A. W. Leenstra, B. de Ronde, J. P. Dehollain, J. T. Muhonen, F. E. Hudson, K. M. Itoh, A. Morello, and A. S. Dzurak, *Nat. Nanotechnol.* **9**, 981 (2014).
- [8] M. Veldhorst, C. H. Yang, J. C. C. Hwang, W. Huang, J. P. Dehollain, J. T. Muhonen, S. Simmons, A. Laucht, F. E. Hudson, K. M. Itoh, A. Morello, and A. S. Dzurak, *Nature (London)* **526**, 410 (2015).
- [9] A. Laucht, J. T. Muhonen, F. A. Mohiyaddin, R. Kalra, J. P. Dehollain, S. Freer, F. E. Hudson, M. Veldhorst, R. Rahman, G. Klimeck, K. M. Itoh, D. N. Jamieson, J. C. McCallum, A. S. Dzurak, and A. Morello, *Sci. Adv.* **1**, e1500022 (2015).
- [10] D. Culcer, L. Cywinski, Q. Li, X. Hu, and S. Das Sarma, *Phys. Rev. B* **82**, 155312 (2010).
- [11] C. H. Yang, A. Rossi, R. Ruskov, N. S. Lai, F. A. Mohiyaddin, S. Lee, C. Tahan, G. Klimeck, A. Morello, and A. S. Dzurak, *Nat. Commun.* **4**, 2069 (2013).
- [12] M. A. Bakker, S. Mehl, T. Hiltunen, A. Harju, and D. P. DiVincenzo, *Phys. Rev. B* **91**, 155425 (2015).
- [13] E. Barnes, J. P. Kestner, N. T. T. Nguyen, and S. Das Sarma, *Phys. Rev. B* **84**, 235309 (2011).
- [14] A. G. Fowler, M. Mariantoni, J. M. Martinis, and A. N. Cleland, *Phys. Rev. A* **86**, 032324 (2012).
- [15] S. J. Angus, A. J. Ferguson, A. S. Dzurak, and R. G. Clark, *Nano Lett.* **7**, 2051 (2007).
- [16] F. J. Ohkawa, *Solid State Commun.* **26**, 69 (1978).
- [17] T. Ando, A. B. Fowler, and F. Stern, *Rev. Mod. Phys.* **54**, 437 (1982).
- [18] V. A. Volkov and T. N. Pinsker, *Surf. Sci.* **81**, 181 (1979).
- [19] F. T. Vasko, *JETP Lett.* **30**, 541 (1979).
- [20] T. Ando and S. Mori, *Surf. Sci.* **113**, 124 (1982).
- [21] M. O. Nestoklon, L. E. Golub, and E. L. Ivchenko, *Phys. Rev. B* **73**, 235334 (2006); L. E. Golub and E. L. Ivchenko, *ibid.* **69**, 115333 (2004).
- [22] M. O. Nestoklon, E. L. Ivchenko, J. M. Jancu, and P. Voisin, *Phys. Rev. B* **77**, 155328 (2008).
- [23] A. L. Saraiva, M. J. Calderón, X. Hu, S. Das Sarma, and B. Koiller, *Phys. Rev. B* **80**, 081305(R) (2009).
- [24] A. A. Kiselev, E. L. Ivchenko, and U. Rössler, *Phys. Rev. B* **58**, 16353 (1998).
- [25] M. Friesen and S. N. Coppersmith, *Phys. Rev. B* **81**, 115324 (2010).
- [26] E. Knill, D. Leibfried, R. Reichle, J. Britton, R. B. Blakestad, J. D. Jost, C. Langer, R. Ozeri, S. Seidelin, and D. J. Wineland, *Phys. Rev. A* **77**, 012307 (2008).
- [27] E. Magesan, J. M. Gambetta, B. R. Johnson, C. A. Ryan, J. M. Chow, S. T. Merkel, M. P. da Silva, G. A. Keefe, M. B. Rothwell, T. A. Ohki, M. B. Ketchen, and M. Steffen, *Phys. Rev. Lett.* **109**, 080505 (2012).
- [28] M. A. Fogarty, M. Veldhorst, R. Harper, C. H. Yang, S. D. Bartlett, S. T. Flammia, and A. S. Dzurak, *Phys. Rev. A* **92**, 022326 (2015).
- [29] N. M. Zimmerman, C. H. Yang, N. S. Lai, W. H. Lim, and A. S. Dzurak, *Nanotechnology* **25**, 405201 (2014).